TRACHEID EFFECT SCANNING AND EVALUATION OF IN-PLANE AND OUT-OF-PLANE FIBER DIRECTION IN NORWAY SPRUCE TIMBER

*A. Briggert**†*
PhD Student
E-mail: andreas.briggert@lnu.se

M. Hu†
Postdoc
E-mail: min.hu@lnu.se

A. Olsson
Professor
E-mail: anders.olsson@lnu.se

J. Oscarsson
Senior Lecturer
Department of Building Technology
Linnaeus University
Växjö, Sweden
E-mail: jan.oscarsson@lnu.se

(Received February 2018)

Abstract. Local fiber direction is decisive for both strength and stiffness in timber. In-plane fiber direction on surfaces of timber can be determined using the so-called tracheid effect which is frequently used in both research and industry applications. However, a similar established method does not exist for measuring the out-of-plane angle, also known as diving angle. The purposes of this article were to evaluate if the tracheid effect can also be used to determine, with reasonable accuracy, the out-of-plane angle in Norway spruce and to verify an existing mathematical model used to calculate the fiber direction in the vicinity of knots. A newly developed laboratory laser scanner was applied for assessment of fiber directions in a single Norway spruce specimen containing a knot. It was assumed that the specimen had a plane of symmetry through the center of the knot, and by splitting the specimen through this plane into two parts, it was possible to make measurements on orthogonal planes. The results showed that the out-of-plane angle could not be determined with very high accuracy and the difficulties related to this objective were analyzed. Regarding the mathematical model of fiber direction in the vicinity of a knot, fiber directions calculated on the basis of this model agreed well with experimentally obtained fiber directions, but successful application of the model requires that the geometry of the knot is known in detail.

Keywords: Diving angle, fiber direction, knots, laser scanning, Norway spruce, tracheid effect.

INTRODUCTION

Timber can be approximated as an orthotropic material, which means that the mechanical properties such as stiffness and strength differ between longitudinal, radial, and tangential direction of the stem. This in turn is related to the fiber direction of the material, ie the direction of the cells. In softwood, one type of cell is present in large numbers; these are called tracheids or fibers. Within a standing tree, tracheids fulfill the functions of transporting nutritious substances and water and providing structural support of the stem (Dinwoodie 2000). In clear wood, the longitudinal direction of the tracheids is, in general, close to parallel with the longitudinal stem direction, but small deviations occur because of spiral grain and taper of the stem. Around imperfections such as knots, tracheids

* Corresponding author
† SWST member

Wood and Fiber Science, 50(4), 2018, pp. 411-429
https://doi.org/10.22382/wfs-2018-053

deviate substantially from the stem's longitudinal direction.

Already Hankinson (1921) presented a mathematical expression, including parameters to be set on the basis of experimental data, for the relationship between strength and fiber direction. The expression implies that even small deviations between the direction of fiber and direction of loading result in a significant reduction of the strength. Later on, a similar relationship between fiber direction and modulus of elasticity was presented (Hatayama 1984).

Based on the known properties of wood as described earlier, it can be concluded that the variation of fiber direction is of great importance for the structural properties of sawn timber. The local fiber direction in the plane of a board surface can be determined using the so-called *tracheid effect*, which means that tracheids in softwood spread concentrated light, such as laser light, better in the fiber direction than across (Matthews and Beech 1976; Åstrand 1996; Nyström 2003). When a circular beam of laser light illuminates a surface of softwood timber, a part of the light will, according to Soest et al (1993), scatter into the cell structure and transmit mainly in the longitudinal direction of the tracheids. When the transmitted light comes to the walls and ends of a cell, a part of that light will be reflected back to the surface and because of the tracheid effect enters a shape that resembles an ellipse, with its major axis oriented as a projection of the fiber's longitudinal direction onto the surface. Examples of the tracheid effect are shown in Fig 1. Figure 1(a) shows a surface of a board of Norway spruce (*Picea abies*). Figure 1(b) displays, for the surface exhibited in (a), the spread of laser light due to illumination by dot laser beams of circular shape.

The tracheid effect has for many years been used in commercial wood scanners as a means to detect defects. However, it is not until recently that the possibility of determining the fiber direction on board surfaces has been applied for the purpose of machine strength grading. In 2015, a new strength-grading method based on tracheid effect

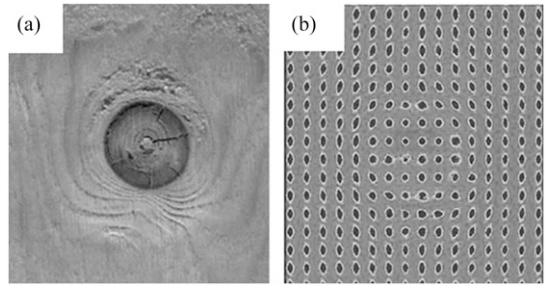

Figure 1. (a) Board surface of Norway spruce with a round knot. (b) The same surface illuminated by circular dot laser beams which, because of the tracheid effect, have entered elliptic shapes on the board surface. Figures from Petersson (2010).

measurements was approved for application on the European market. The method is presented in detail in Olsson et al (2013) and can be summarized as follows: based on knowledge of the fiber direction on board surfaces, together with weight, dimension, and first axial dynamic resonance frequency, a profile of a board's bending modulus of elasticity is calculated. The lowest value along this profile is applied as indicating property (IP) to strength. For a sample of more than 900 pieces of timber of Norway spruce, the coefficient of determination (R^2) between the described IP and bending strength was as high as 0.69 (Olsson and Oscarsson 2017). For comparison, the R^2 between bending strength and axial dynamic modulus of elasticity, the latter being a common IP of machine strength grading, was for the same sample 0.53. Data of tracheid effect measurements, together with data of X-ray scanning, were also used by Viguier et al (2017) as components of another suggested IP to bending strength. For a sample of 437 spruce boards, the application of this IP resulted in an R^2 of 0.66.

The grading methods based on knowledge of local fiber direction are based on several assumptions, of which one of the more important is that the in-plane component of the fiber direction on the board's longitudinal surfaces is assumed to represent the actual fiber direction both on the surface of the board and in the interior of the board. The out-of-plane component of the fiber direction on surfaces is thus ignored, since it is

not as easily determined as the in-plane component. However, the actual three-dimensional (3D) fiber direction, particularly in the close surroundings of knots, has a considerable effect on the mechanical properties of sawn timber, and efforts should be made to collect data also of the out-of-plane component of the fiber direction to enable more accurate assumptions of fiber direction of the timber. It is likely that success in this respect would lead to even more accurate machine strength grading than what is presently obtained.

Several researchers have investigated the fiber direction in the vicinity of knots. A qualitative study on how fibers integrate at a branch–stem junction was presented by Shigo (1997), and a mathematical approach for description of 3D fiber direction around knots was suggested by Foley (2003). The latter is based on the so-called grain flow analogy aiming at capturing the tangential-longitudinal fiber direction around knots, together with a mathematical expression describing the radial-longitudinal fiber direction. The grain flow analogy was first introduced by Goodman and Bodig (1978) and then further developed by Philips et al (1981). A more detailed description of the radial-longitudinal mathematical expression is given in the mathematical expression section. A similar mathematical approach as the one suggested by Foley (2003) has been implemented for use in combination with a 3D finite element model of timber (Lukacevic and Füssl 2014). Hu et al (2017) is one of few studies that has presented detailed experimental data of growth layers and fiber directions in 3D in the vicinity of a knot in Norway spruce. Other results from the same investigation were presented by Briggert et al (2016a) and the present article is also a result of the same laboratory work.

As regards the determination of the out-of-plane angle of the fiber direction on surfaces, the possibility of extracting such information from dot laser illumination of wood surfaces has been investigated. Simonaho et al (2004) proposed that the out-of-plane angle (also known as diving angle) of illuminated fibers could be assessed by considering the shape of the reflected laser light on the surface. The idea was that fibers with larger diving angle reflect less light back to the board surface than what fibers with smaller diving angle do. As a result, the elliptically shaped light on the surface becomes more circular as the diving angle increases. This was captured by the length ratio, below referred to as the *shape factor ratio*, between the minor and major axis of the ellipse. The procedure that Simonaho et al (2004) applied to establish a mathematical relationship between this ratio and the diving angle can be summarized as follows: 1) Twenty clear wood specimens, 10 of silver birch (*Betula pendula*), and 10 of Scots pine (*Pinus sylvestris* L.) were sawn so that each specimen contained fibers with identical diving angle to the investigated surface. For both species, the angles ranged from 0 to 90°, with increments of 10°. Each specimen was then illuminated by a dot laser in a predefined grid, and for each illumination, a camera was used to capture the corresponding shape of the reflected light. The grid size used for all specimens was 5×5 mm^2, with steps of 1 mm in each of the two orthogonal directions of the grid. This implied that the camera images were used for the determination of shape factor ratios in 36 positions on each specimen. 2) The data were then analyzed statistically with the purpose of determining a mathematical expression describing the relationship between diving angle and shape factor ratio. The established relationship is represented by the solid curve in Fig 2. Furthermore, the derived mathematical expression was verified by the application of a further specimen containing a single knot and cut so that tangential-longitudinal and radial-longitudinal surfaces, respectively, were exposed. Shape factor ratios were then measured close to one edge of a tangential-longitudinal surface, and corresponding in-plane angles were measured close to the same edge but on the adjacent radial-tangential surface. Because an in-plane angle measured on a radial-longitudinal surface corresponds to the diving angle on a tangential-longitudinal surface, the accuracy of the diving angles predicted on the basis of the relationship shown in Fig 2 could be assessed. The data obtained by these measurements resulted in an R^2 of 0.91 between shape

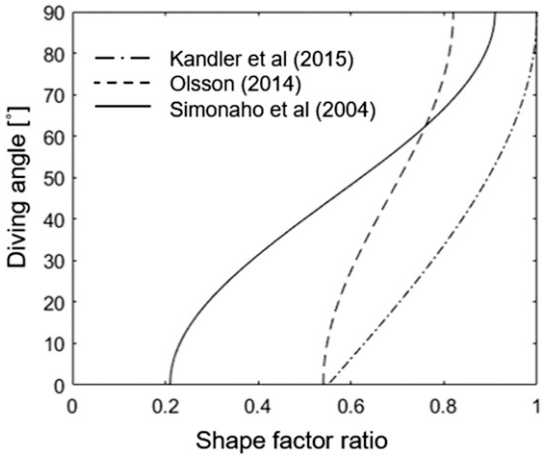

Figure 2. Suggested mappings between shape factor ratio and diving angle. Simonaho et al (2004) investigated birch and pine. Olsson and Oscarsson (2014) and Kandler et al (2015) both investigated Norway spruce.

factor ratios and diving angles. Simonaho et al (2004) thus concluded that the diving angle on surfaces of silver birch and Scots pine can be identified using dot laser illumination, ie determined as a function of the shape factor ratio. However, no scatter plot showing the relationship was presented for the specimen containing a knot.

Olsson and Oscarsson (2014), Kandler et al (2015), Briggert et al (2016b), and Hu et al (2016) used the method suggested by Simonaho et al (2004) to determine the out-of-plane angle and to calculate the 3D fiber direction on surfaces of boards of Norway spruce. In two of these investigations, Olsson and Oscarsson (2014) and Kandler et al (2015), new relationships between shape factor ratio and diving angle were derived. The relationships that were established are represented by dashed and dashed-dotted curves, respectively, in Fig 2. In this context, it should be noted that the same equipment, a commercial scanner of make WoodEye 5 (WoodEye, Linköping, Sweden) available at the laboratory of Linnaeus University, was used in both of these investigations to sample data. As regards the investigations carried out by Briggert et al (2016b) and Hu et al (2016), the relationship determined by Olsson and Oscarsson (2014) was used. In Fig 2, it is clearly shown that the two relationships for Norway spruce differ, even though the same wood scanner was used. For example, for a specific laser illumination, the shape factor ratio was calculated to be 0.8. The mathematical expression derived by Olsson and Oscarsson (2014) results in a diving angle of 75-80°, whereas the one derived by Kandler et al (2015) results in an angle of approximately 30-35°. This implies an uncertainty of the relationship between shape factor ratio and diving angle of Norway spruce timber. Therefore, the strength of this relationship needs to be thoroughly investigated.

Purpose and Aim

The overall purpose of this research was to contribute to knowledge and development of methods to determine, nondestructively and in a practical way, the 3D fiber direction of timber, especially in the surroundings of knots. This is motivated by the possible application of such knowledge for development of accurate methods for machine strength grading of timber. The purpose can be divided into two particular aims:

1. Investigate, for Norway spruce timber, the relationship between the shape of reflected light, ie of a grayscale image of reflected light, of an illuminated wood surface and the diving angle of the fibers at the surface.
2. Validate the model for the radial-longitudinal fiber direction in the vicinity of knots presented by Foley (2003) and discuss the potential applicability and limitations of this model for engineering purposes.

The research required equipment, using the tracheid effect, to determine the fiber direction on timber surfaces with both high precision and accuracy. Because such equipment was not available, another and initial objective was to develop a laboratory scanner for this purpose.

DEVELOPMENT AND FUNCTION OF LABORATORY SCANNER

Equipment

To be able to carry out the research presented in this article, a self-developed laboratory scanner

was applied. This scanner, which is exhibited in Fig 3, consists of the so-called *XYZ*-table including a stationary table and a movable frame. On the latter, a dot laser, a camera, and a microscope are installed. The frame is movable in the longitudinal direction of the stationary table, ie in the *y*-direction of the coordinate system defined in Fig 3. Laser, camera, and microscope are installed on the frame in a way that makes them movable transversely and vertically in relation to the mentioned table, ie in *x*- and *z*-directions. The installed equipment can, therefore, be moved in three orthogonal directions. By means of computer software, it is possible to maneuver frame and equipment to predetermined coordinates or in a predefined grid. The board surface can, thus, be illuminated by the dot laser, at one defined position at the time. High-resolution pictures simultaneously taken by the camera provide knowledge about the laser light that is reflected from the wood surface. The smallest movement possible in any of the three orthogonal directions is 0.031 mm.

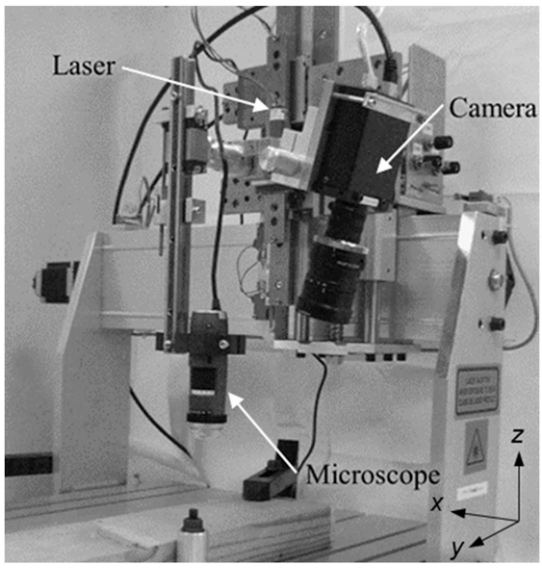

Figure 3. Self-developed laboratory scanner including stationary table, moveable frame, dot laser, camera, and microscope. To avoid movements of a measured specimen during repositioning of the frame or the installed equipment, the investigated wood specimen is fastened to the stationary table.

The laser, which is of the make Acculase, has a wavelength of 785 nm and has similar characteristics as the one used in the commercial wood scanner WoodEye 5. When focused and directed toward the camera sensor, the shape of the laser spot is *close* to circular and its diameter is approximately 0.2 mm. The camera is of grayscale type with a resolution of 1024 × 2048 pixels and it is of the same make and model as the camera used in WoodEye 5. Regarding the microscope, which is of make Dino-Lite, it has a magnification range of 10×-140× which makes it possible to carry out microscopic investigations of board surfaces. Figure 4(a) and (c) show images taken by the camera and the microscope, respectively.

Image Processing

A grayscale image is a two-dimensional array having the number of rows and columns equivalent to the number of pixels of the applied camera's sensor. As mentioned earlier, a grayscale camera with a sensor of 1024 × 2048 pixels was installed on the laboratory scanner. The function of a sensor is to measure the amount of light that is reflected by an object and to associate an intensity value to each element, ie to each pixel, of the array. The sensor installed in the camera applied in this investigation had a range of intensity values between 0 and 255. A value of 255 corresponds to the color of white, whereas a value of 0 corresponds to the color of black.

As shown in Fig 3, the laser on the laboratory scanner was installed perpendicular to the scanned surface, ie the direction of the laser beam was parallel with the normal direction of the investigated surface. As for the camera, it was installed at a target rotation angle of 15° around the *y*-axis, see Fig 3, but because of occasional reflexions occurring in the measurement setup, the angle was in some measurements adjusted with a few degrees. Because of the described rotation angle, camera pictures displayed a projection of the reflected light on the investigated surface. To achieve information corresponding to a camera installed with a rotation angel of

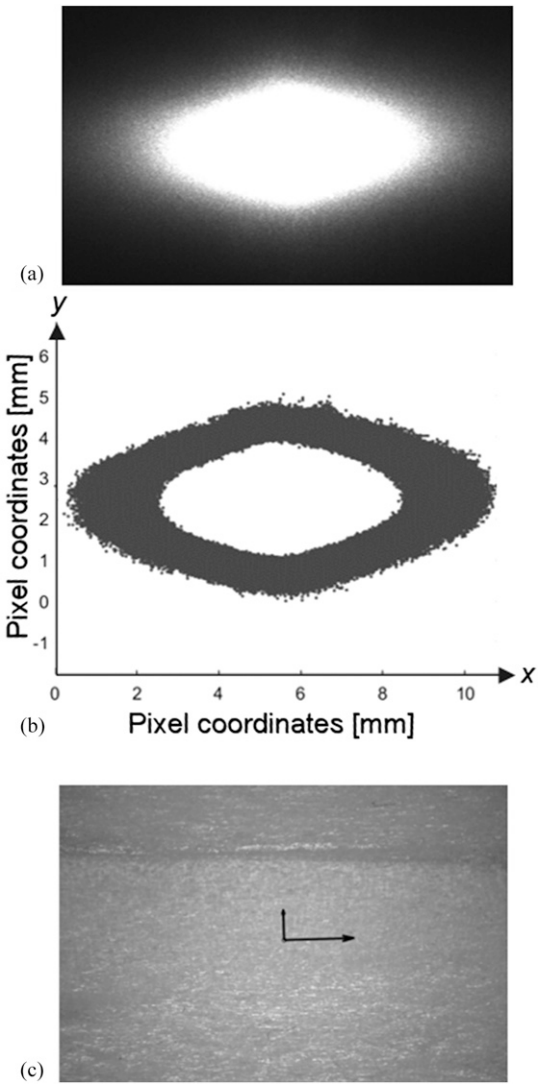

Figure 4. (a) Photograph showing the reflected laser light on a Norway spruce surface. (b) Scatter (blue color) of pixel coordinates in (a) having an intensity level between 50 and 150. The size of the analyzed light scatter is approximately 10 × 5 mm in the fiber direction and in the transverse direction, respectively. (c) Microscopic image of the same surface as exhibited in (a). Direction and length of the arrows correspond to the eigenvectors and eigenvalues, respectively, of the scatter in (b). The longest arrow follows the in-plane direction of the illuminated fibers.

0° around the *y*-axis, the viewing perspective of the pictures was compensated for by elongating the distances between the picture's pixel coordinates in the *x*-direction. The elongation was calculated as

$$P_A = \frac{P_O}{\cos(\alpha)}, \quad (1)$$

where P_A is the adjusted pixel coordinate, P_O is the pixel coordinate originally identified by the rotated camera, and α is the rotation angle of the camera. Consequently, changing a picture according to Eq (1) resulted in the picture being displayed as if the camera was installed parallel to the laser, ie perpendicular to the investigated surface.

It was found during the investigation that to capture the tracheid effect, the maximum intensity of 255 of the grayscale image had to be reached for a certain area of the reflected light, ie a part of the picture had to be saturated. When eg infrared filters were used to decrease the intensity below the maximum level of 255, the light that was spread in the longitudinal fiber direction was reduced to such an extent that the laser dots took a more circular shape. This resulted in the tracheid effect being difficult to discern and unreliable to use as a tool for determining the fiber direction. A disadvantage using a high light intensity, on the other hand, is that the reflected light used to determine the fiber direction covers a quite large area of the wood specimen which results in a rather low resolution of determined fiber directions.

Figure 4(a) shows a part of a grayscale picture taken by the camera installed on the laboratory scanner. The shown part of the picture displays the reflected light from a wood surface when illuminating it with the dot laser. Here, it can be seen that the intensity of light in such a picture varies; it is at the highest in the central part of the dot and typically decreases with distance from its center. To determine the direction of the major and minor axes, respectively, of the reflected light, threshold values have to be set for the intensity. In this investigation, a high threshold value of 150 and a low threshold value of 50 were used. The former was set so that the saturated part of the pictures was disregarded in the calculations because this part of the picture could be affected by the shape of the laser spot. The lower threshold value of 50 was used to remove the parts of the

picture that were black. Then, by defining a coordinate system, see Fig 4(b), and identifying coordinates for pixels in which the light intensity was within the set range of intensity levels, images were analyzed by means of a scatter of the data. Figure 4(b) shows the scatter corresponding to the picture in Fig 4(a), for the set threshold values. Furthermore, the two eigenvectors and the two eigenvalues associated with the covariance matrix, calculated from such a scatter, correspond to the directions and lengths, respectively, of minor and major axes of the reflected light. The covariance matrix is defined as

$$\boldsymbol{C} = \begin{bmatrix} \mathrm{Var}(x,x) & \mathrm{Cov}(x,y) \\ \mathrm{Cov}(y,x) & \mathrm{Var}(y,y) \end{bmatrix}, \qquad (2)$$

where Var(x,x) is the variance of x-coordinates for pixels in which the light intensity was within the set range of intensity levels, Var(y,y) is the corresponding variance of y-coordinates, and $\mathrm{Cov}(x,y) = \mathrm{Cov}(y,x)$ is the corresponding covariance. The eigenvectors and eigenvalues are calculated by

$$\boldsymbol{C} \cdot \mathbf{v} = \lambda \cdot \mathbf{v}, \qquad (3)$$

where $\mathbf{v}$ is an eigenvector and λ the corresponding eigenvalue. Eq (3) has two solutions, ie two different values of λ and corresponding eigenvectors that fulfill the equation. The low and the high values of λ that solve the equation are denoted as λ_1 and λ_2, respectively, and the corresponding eigenvectors are denoted as $\boldsymbol{v}_1$ and $\boldsymbol{v}_2$, respectively. The fiber direction in the investigated plane is represented by the vector $\boldsymbol{v}_2$. The diving angle is a function of the shape factor ratio, s, which is defined as

$$s = \frac{\lambda_1}{\lambda_2}. \qquad (4)$$

Figure 4(c) shows a microscope image of the same surface as illuminated in (a). The direction of the calculated eigenvectors of the scatter shown in (b) is indicated by the direction of the arrows, whereas the length of the arrows corresponds to the calculated eigenvalues. The longest arrow follows the in-plane direction of the illuminated fibers.

MATERIAL FOR ASSESSMENT AND SCANNING PROCEDURE

Preparation of Wood Specimen

The wood material used in this investigation was chosen from a tree of Norway spruce harvested at the locality of Kråkenäsryd Gårdsby (56°57′17″N, 14°54′06″E) in southern Sweden. Details of the well-documented stand from which the tree was selected are given in Hu et al (2017). A specimen with the shape of a rectangular solid displaying a round knot was cut from the selected tree, see Fig 5. When preparing the specimen, a plane of symmetry, indicated by the dashed lines in Fig 5, was aimed for through the knot. This meant that the solid was cut so that the pith of the knot was positioned in the symmetry plane. The pith of the tree, indicated in Fig 5, was also positioned in the symmetry plane, and the longitudinal direction of this pith was parallel with the longitudinal direction of the solid. The dimension of the solid after drying to 17% MC and final adjustment/planing was 95 × 559 × 105 mm in tangential, longitudinal, and radial directions, respectively. Usually, Norway spruce specimens used in scientific investigations are dried to 12% MC, but to avoid crack propagation, drying was here aborted at 17%.

Because a plane of symmetry through the pith of the knot was assumed to exist, splitting of the specimen into two parts, through the intended plane of symmetry, resulted in two specimen parts assumed to be mirrored versions of each other, see Fig 6.

Scanning Procedure

As described in the last paragraph of the previous section, the specimen shown in Fig 5 was split through an assumed plane of symmetry, resulting in two parts as shown in Fig 6. The part of the specimen shown in Fig 6(a) was scanned for assessment of fiber direction on radial-longitudinal planes, ie on yz-surfaces (see defined coordinate

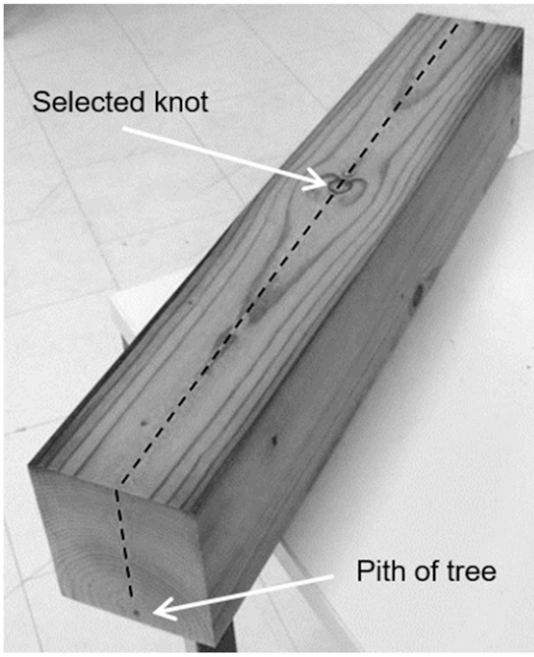

Figure 5. The specimen after drying and planing. The dashed line illustrates the assumed plane of symmetry, in which both the pith of the knot and the pith of the tree were assumed to be positioned.

system in Fig 6). The first scanning of this part was thus performed on the surface displaying the splay knot. The part was then planed so that 2 mm was removed in the negative *x*-direction before a new *yz*-surface was scanned and then another 2 mm was removed in the negative *x*-direction, followed by scanning, and so on. As regards the other part, shown in (b), it was scanned for assessment of fiber direction on tangential-longitudinal planes, ie on *xy*-surfaces. The first scanning of this part was carried out on the surface showing the cross section of the splay knot, ie on the *xy*-surface shown in Fig 6(b). Planing of this part was performed in the negative *z*-direction and repeated laser scans were performed on *xy*-surfaces 2 mm apart, ie 2 mm was removed by planing after each scanning.

On each scanned plane on each of the two parts obtained after splitting, grids of 2 × 2 mm and 4 × 4 mm, respectively, were employed for the dot laser scanning. The finer grid was used for the knot itself and its close surroundings and the coarser one was used outside this area. For the part displaying the splay knot (shown in Fig 6[a]), the low and high resolution areas on the *yz*-surfaces were 264 × 96 mm and 140 × 96 mm, respectively. For the other part (shown in Fig 6[b]), the low and high resolution areas were on the *xy*-surfaces 40 × 264 mm and 40 × 140 mm, respectively.

For all scanned planes, on both parts shown in Fig 6, the same start and stop positions of the 4 × 4 mm grids were used in the *y*-direction. Furthermore, relying on the assumption of the plane

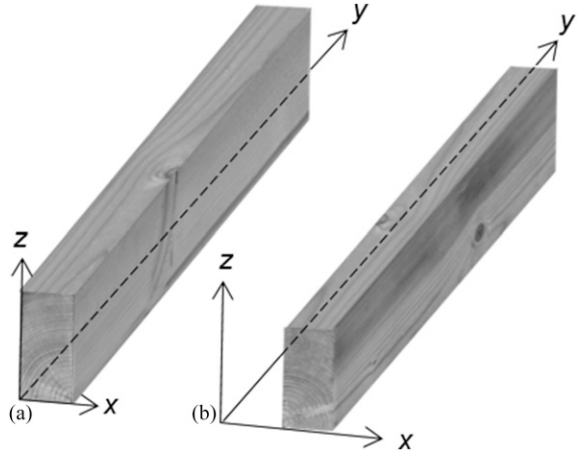

Figure 6. The specimen was split along the assumed plane of symmetry, resulting in two parts being mirrored versions of each other.

of symmetry, the grids, and the successive planing of the two parts of the specimen, were arranged such that the laser dots were focused in the same positions/coordinates in 3D space. As a result, for each position in the 3D grid, the in-plane fiber direction together with the corresponding shape factor ratio was identified on two different surfaces orthogonal to each other. Similar arrangements, but with an offset to the 4×4 mm start and stop positions, were applied for the 2×2 mm grid.

DOT LASER IMAGES AND FIBER DIRECTIONS

Determination of In-Plane Fiber Direction

For every illuminated point in the grid on a surface, both the in-plane fiber direction and the shape factor ratio were calculated according to Eqs (1-4). The photograph in Fig 7(c) shows the first scanned radial-longitudinal surface of the part of the specimen displayed in Fig 7(a). Note that both the pith of the knot and the pith of the tree are visible in Fig 7(c), which confirms that the specimen was successfully split through the knot. The photograph in Fig 7(d) shows one of the tangential-longitudinal surfaces scanned, ie one of the scanned surfaces of the part of the specimen shown in Fig 7(b). The plane shown in Fig 7(d) is positioned approximately 50 mm from the pith of the tree, ie at a radial distance from the pith where the knot was still alive. Plotted on the photographs in Fig 7(c) and (d) are the determined in-plane fiber directions, represented by short black lines. Both surfaces displayed in Fig 7(c) and (d) are within the high resolution, 2×2 mm, grid. The range in y-direction is the same for both surfaces.

In the main parts of the areas showing the pith of the knot on the radial-longitudinal surface, see Fig 7(c), the detected in-plane fiber direction deviates from the direction of the pith and the

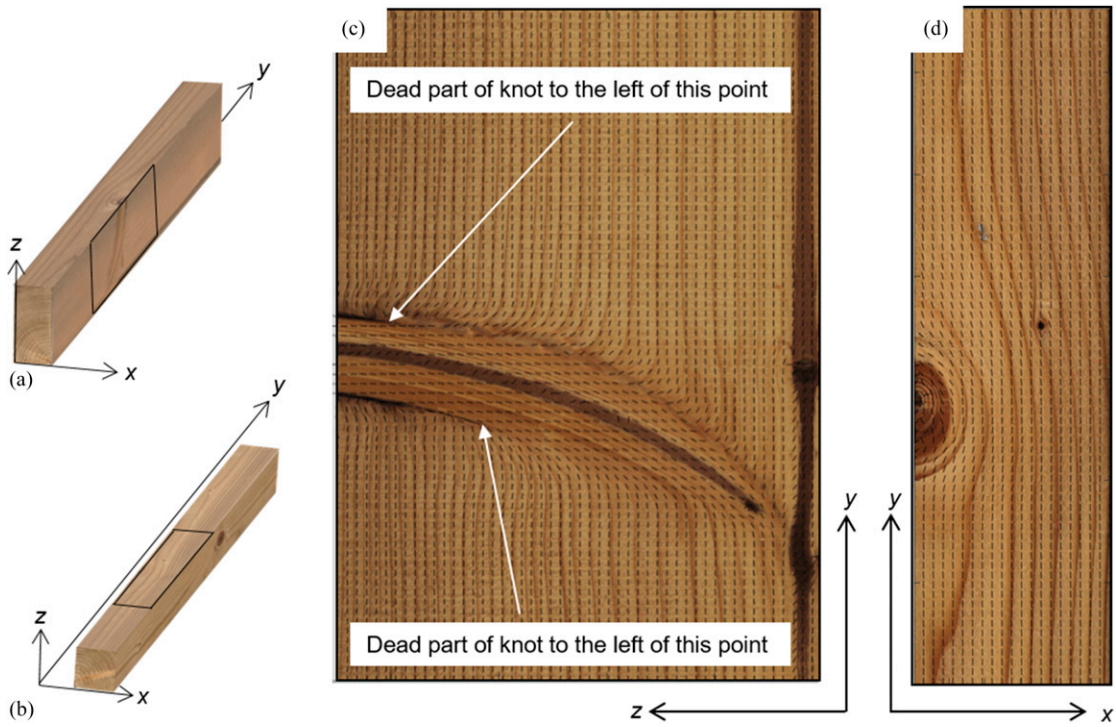

Figure 7. (a) and (b) show the two parts of the specimen. The black rectangles drawn on the surfaces correspond to the surfaces displayed in (c) and (d). (c) Photograph of a radial-longitudinal plane, and (d) photograph of a tangential-longitudinal plane. Calculated in-plane fiber direction is shown by the short black lines.

direction of grain close to the pith. This shows that when the dot laser illuminates the pith itself, there is no tracheid effect to rely on because the material of the pith does not consist of tracheids. Outside these small areas, however, the determined fiber directions seem to coincide very well with the actual fiber direction. An observation that can be made by considering Fig 7(c) is that the transition zone from clear wood fibers to knot fibers is rather small, at its largest 8-10 mm. In the area where the knot is dead, ie in areas to the very left in Fig 7(c), the in-plane direction of fibers just outside the knot is almost perpendicular to the direction of the knot itself. This is because fibers here do not integrate with the knot but actually grow around it.

On the tangential-longitudinal surface shown in Fig 7(d), it is clear that fibers in the vicinity of a live knot also grow around it. Inside the knot, the determined fiber direction is more or less random. Laser spots, when illuminating a surface of a cross section of a round knot, are almost circular in shape. This is not very surprising because most of the laser light transmits mainly in the longitudinal direction of the fibers, which in a cross section of a round knot is directed perpendicular to the surface itself.

Investigation of Out-of-Plane Fiber Direction

Figure 8 shows color plots representing shape factor ratios, calculated using Eq (4), over the same wood surfaces as shown in Fig 7(c) and (d). Figure 8(a) shows the radial-longitudinal surface, and here, it can be seen that the shape factor ratios are at its highest at the knot boundary and inside the pith of the knot and the pith of the tree. Outside of these areas, ie inside the remaining part of the visible knot surface and in clear wood, the shape factor ratios are significantly lower. This is because of the fact that the longitudinal direction of fibers at such a knot surface and within clear wood generally is directed in the plane of such surfaces. In Fig 8(b), on the other hand, it can be seen that shape factor ratios on a tangential-longitudinal surface become at its

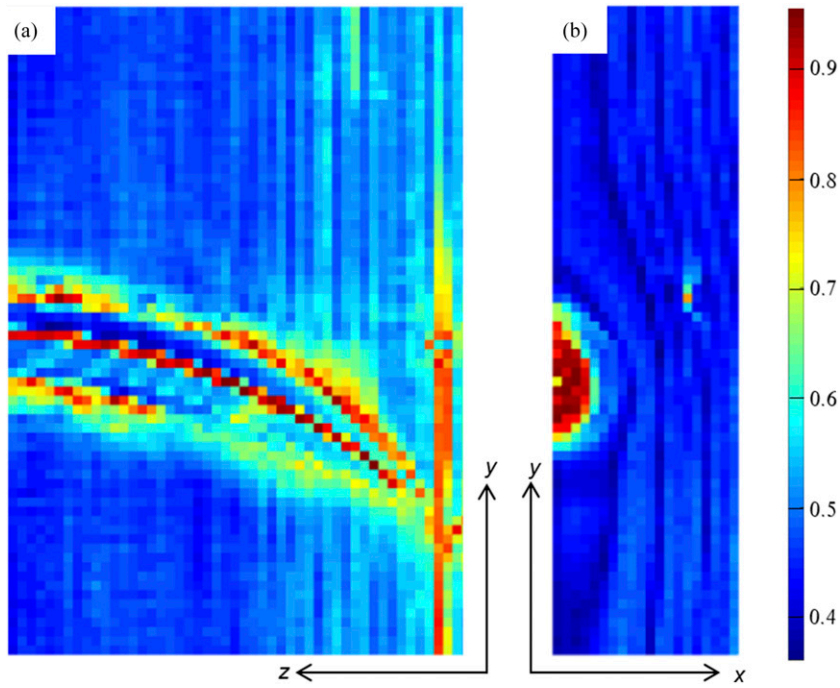

Figure 8. Color plots of shape factor ratios determined by Eq 4, for the surfaces shown in Fig 7(c) and (d), respectively.

highest inside the knot. In clear wood areas, the shape factor ratios are at its lowest, and there is a visible transition between clear wood and knot, from low shape factor ratios in clear wood to high shape factor ratios inside the knot. Another observation is that the shape factor ratios differ in clear wood between earlywood and latewood. Here, the shape factor ratios are lower in latewood than in earlywood. Because of limitations of the resolution obtained, a corresponding annular ring pattern cannot be clearly identified on the radial-longitudinal surface displayed in Fig 8(a). The shape factor ratios displayed in Fig 8(a) and (b) are also influenced by threshold values used in the analysis of the laser spot, see the Image Processing section. Different limits of the threshold values would result in somewhat different shape factor ratios.

The experimental campaign presented herein was designed with the purpose of providing a more reliable assessment of the relationship between shape factor ratio and diving angle for Norway spruce than what has been achieved in earlier investigations. Relying on the assumption of symmetry, as explained earlier and illustrated in Figs 5 and 6, the same position in 3D space could be investigated by laser scanning in two orthogonal planes; the diving angle determined on the basis of the shape factor ratio on one plane could be compared with the in-plane fiber angle on the perpendicular plane. The determined in-plane angle should, if the applied models for shape factor ratio and diving angle are perfectly calibrated, be identical with the diving angle on the plane where the shape factor ratio was assessed. Consequently, two different comparisons/mappings could be performed. In one of them, the shape factor ratio was determined on the *xy*-plane (cf. Fig 7[b]) and the in-plane angle was determined in the same 3D position but on the *yz*-plane (cf. Fig 7[a]). In the other comparison/mapping, the shape factor was determined on the *yz*-plane and the in-plane angle was determined on the *xy*-plane. In this article, the first of the two mappings, ie the one with the shape factor being determined on the *xy*-plane, is reviewed more thoroughly than the other one.

For assessment, a total of 2 *yz*- and 14 *xy*-planes were used. These planes were positioned so that 28 different intersections between these orthogonal planes were achieved in the *y*-direction. Each such intersection is from here on referred to as a scanning line. Along each such line, a total number of 71 positions in *y*-direction, 2 mm apart, were examined using dot laser and camera, see Fig 7(c) and (d).

Figure 9(a) and (b) show, for positions along two different scanning lines, the relationship between the measured in-plane angle on the radial-longitudinal surface (the *yz*-plane) and the corresponding shape factor ratio, multiplied by 100, measured on the tangential-longitudinal surface (the *xy*-plane). The results shown in Fig 9(a) emanate from a scanning line positioned in a region where the knot is dead, whereas the results exhibited in Fig 9(b) originate from a scanning line in a region where the knot is alive. Both the in-plane angle and the corresponding shape factor ratio are displayed on the vertical axis in Fig 9(a) and (b). On the horizontal axis, the *y*-coordinate of the scanned specimen part is displayed. The zero coordinate in the two figures corresponds to the starting point of the scanning lines, respectively. The boundaries of the knot along the scanning lines are marked with green vertical lines. The asterisks along the curves mark the *y*-coordinate of the positions investigated.

In Fig 9(a) and (b), it is clearly shown that both the shape factor ratios and the corresponding in-plane angles (ie diving angles for the measured shape factor ratio) are at their lowest in clear wood areas. For an in-plane angle lower than 5°, the corresponding shape factor ratio is between 0.4 and 0.5 for both scanning lines, see both (a) and (b). Inside the knot, both the shape factor ratio and the corresponding in-plane angle are, generally, at their highest values. The points located in the transition zone between clear wood and knot show a transition from low to high values for both shape factor ratio and for the corresponding in-plane angle, but there is a variation in the relationship between the two quantities. When laser dots illuminate wood at the boundaries of the knot, fibers within and outside

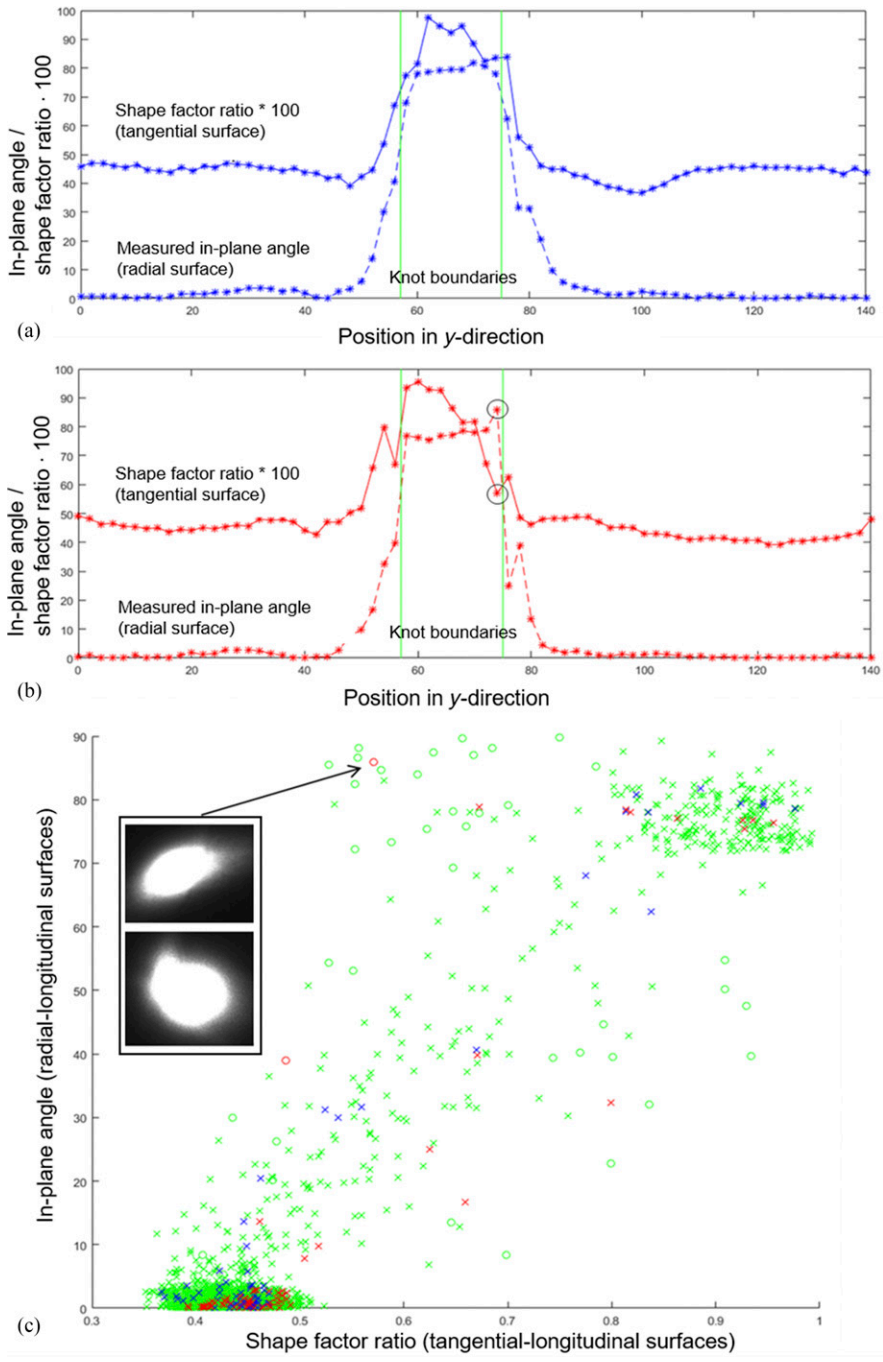

Figure 9. (a) and (b) measured in-plane angle for a radial-longitudinal surface and then calculated shape factor ratio (multiplied by 100) for the corresponding tangential-longitudinal surface determined at positions along two different scanning lines. Such a line is defined as an intersection between an *xy*-plane and *yz*-plane. The asterisks indicate the *y*-coordinates of the investigated positions. Vertical green lines indicate knot boundaries. (c) Scatter plot of all investigated positions along the 28 scanning lines. The two photographs show the laser spots used for assessment of the shape factor ratio (top) and the in-plane angle (bottom) for the point marked by the red circle to which the inserted arrow aims. In (b), this point is marked by two black circles.

the knot reflect light. At these positions, the shape of the reflected light on the surface does not resemble an ellipse. One example of such a position/measurement is marked by the black circles in Fig 9(b) and by the red circle to which the arrow in Fig 9(c) is aiming. The spread of light on the two perpendicular surfaces in this position is shown by the two photographs infolded in Fig 9(c). The top photograph shows the light spot on the tangential-longitudinal (*xy*) surface, ie the light spot used for assessment of the shape factor ratio. The lower photograph shows the light spot on the radial-longitudinal (*yz*) surface, ie the light spot used for assessment of the in-plane angle, which is equivalent to the diving angle on the tangential-longitudinal surface.

Figure 9(c) shows, for all positions along all 28 investigated scanning lines, the relationship between the shape factor ratio on the *xy*-plane and the in-plane angle on the *yz*-plane, each mark representing a unique position in 3D space. Blue marks represent the scanning line displayed in (a) and red marks represent the scanning line displayed in (b). Green marks in (c) represent the remaining scanning lines. The points marked by circles are points where the laser spot is not actually shaped as an ellipse, as eg the one shown in the infolded lower photograph. Identification of nonelliptically shaped laser spots was performed visually. The points marked with crosses represent light spots being close to elliptic in shape.

On the horizontal axis in Fig 9(c), the shape factor ratio of position investigated on the tangential-longitudinal surfaces is given, whereas on the vertical axis, the corresponding in-plane angle for the radial-longitudinal surfaces, ie the diving angle for the tangential-longitudinal surfaces, is given. Here, it can be seen that the spread of the scatter is rather large. For example, if an illuminated point has a shape factor ratio of 0.55, the corresponding diving angle could take on any value between 10 and 88°. One of the reasons for the large spread in the scatter is that the size of elliptically shaped spots of reflected light differs between latewood and earlywood.

Applying linear regression for the relationship between shape factor ratio and diving angle, the coefficient of determination, considering all the data points represented in Fig 9(c), is $R^2 = 0.88$ and $R^2 = 0.92$ if only the points marked by crosses are considered, which is similar to the regression result presented by Simonaho et al (2004) for a specimen of Scots pine containing a knot. However, the high R^2 obtained herein depends on the fact that many data points represent clear wood (where shape factor ratios and diving angles are small) and knot material (where shape factor ratios and diving angles are large). Thus, a high R^2 is obtained even though the scatter is large in the transition zone between the clear wood and the knot. Simonaho et al (2004) do not present a scatter plot for their investigation that corresponds to Fig 9(c) herein.

If instead the opposite relationship as the one shown in Fig 9(a) is investigated, ie if the relationship between the shape factor ratio for the points on the radial-longitudinal plane and the in-plane angle for the tangential-longitudinal surface is investigated, the result shown in Fig 10 is achieved. In this figure, it can be seen that both the shape factor ratio and the corresponding in-plane angle increase in the transition zone of the knot, similar to what is shown in Fig 9(a) and (b). However, inside the knot, the relationship becomes random and irrelevant. This is a consequence of the fact that fibers here are actually directed perpendicular to the tangential-longitudinal surface, and therefore the shape of the ellipses becomes close to circular in this area. Any *identified* in-plane components of the fiber direction of the tangential-longitudinal surface inside the knot area is thus a result of randomness/measurement noise.

MATHEMATICAL EXPRESSION FOR THE RADIAL-LONGITUDINAL FIBER DIRECTION IN THE VICINITY OF KNOTS

As described in the introduction, Foley (2003) presented a mathematical approach for determining the 3D fiber direction in the vicinity of knots. This approach consisted of making use of the so-called flow-grain analogy together with mathematical equations describing the fiber direction in radial-longitudinal planes. In this chapter, the fiber direction, calculated on the basis

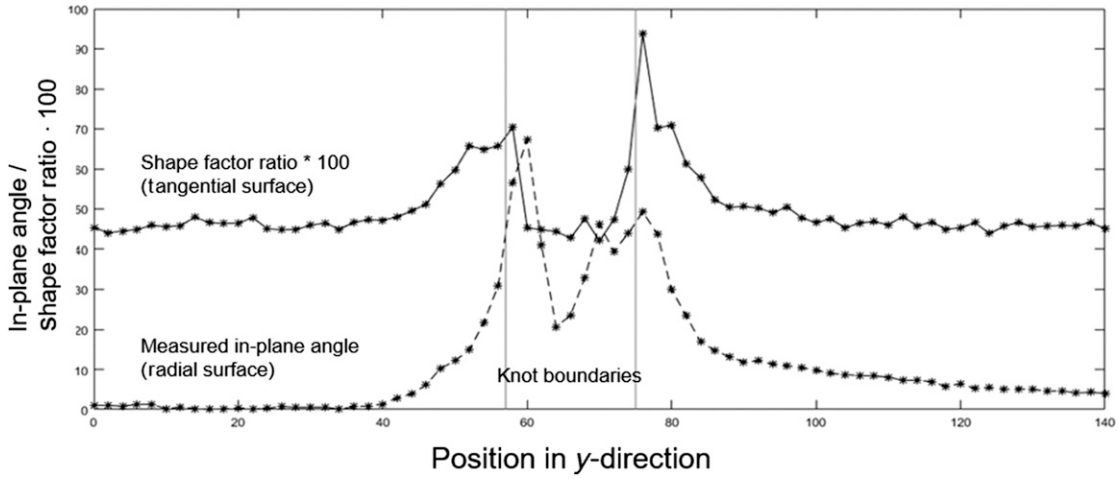

Figure 10. The relationship between shape factor ratio calculated for illuminated points on the radial-longitudinal surface and the in-plane angle calculated for illuminated points on the tangential-longitudinal surface, ie the opposite relationship as the one shown in Fig 9(a).

of the equation valid in the vicinity of a live knot, is compared with the data sampled by the laboratory scanner. However, before such a comparison can be carried out, the boundary of the investigated knot must be defined because the position of the center of the knot at a radial distance from the pith of the tree is essential for the calculations. The definition used in this article for the knot boundary is given in the following section. In the Fiber Direction section, the fiber direction calculated using Foley's equation and the corresponding fiber direction measured using the laboratory scanner are compared for a single radial-longitudinal plane. In the research presented in this article, only the radial-longitudinal surface displaying both the pith of the knot and the pith of the tree, ie the surface plane shown in Fig 7(c), were investigated.

Knot Boundary in the Radial-Longitudinal Plane

The boundary of the knot on the investigated radial-tangential plane was determined by using both a photograph of the surface and the fiber direction measured in the grid defined over the same surface, see Fig 11. For a certain z-coordinate, ie for a certain coordinate in the radial direction, y-coordinates of the upper and lower knot boundaries was defined so that the fiber direction measured at grid positions within the knot deviated less than 10° from the direction of the pith of the knot at the same z-coordinate. The threshold value of 10° was determined after comparison of calculated boundaries corresponding to different threshold values (drawn on top of the photograph) and the photograph of the knot.

Equations describing the upper and the lower knot boundary, respectively, were then determined by fitting polynomials to the y-coordinates determined using the threshold value described in the previous paragraph. For the boundary below the knot, a second-order polynomial was used, whereas a polynomial of third order was applied for the boundary above the knot. The obtained equations of the knot boundaries are illustrated by the blue lines in Fig 11.

Fiber Direction in the Radial-Longitudinal Plane

The fiber direction in the radial-longitudinal plane in the vicinity of a *live* knot can, according to Foley (2003), be determined by first expressing mathematically a distance R between the pith of the log and a certain growth layer and then to

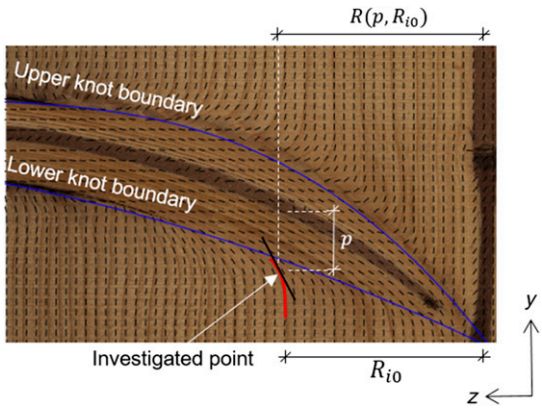

Figure 11. Photograph of splay knot for which knot boundaries were investigated. The blue lines illustrate the polynomial expressions for the boundary of the knot. The smaller black lines show fiber direction measured using the laboratory scanner. The figure also illustrate geometric interpretations of p, R_{i0}, and $R(p, R_{i0})$, which are used in Eq (5).

calculate the fiber direction as the *tangent* of the function of R. The distance R from the pith of the tree to the growth layer is calculated as

$$R(p, R_{i0}) = R_{i0} + A_{\text{bump}} \cdot R_{i0}{}^{A_{\text{exp}}} \cdot p^{-B_{\text{bump}}}, \quad (5)$$

where R_{i0} is the distance in z-direction between the pith of the tree and a position of the same growth layer at some distance from the knot where the fibers are undisturbed by it and p is the distance in y-direction between the center of the knot and the investigated point. Figure 11 displays the geometrical interpretation of $R(p, R_{i0})$, R_{i0}, and p. The values of the parameters A_{bump}, A_{exp}, and B_{bump} are set empirically and depend on species and knot geometry. In this investigation, these parameters were set in agreement with what Foley (2003) suggested for Norway spruce. Based on Eq (5), the shape of growth layer surfaces is thus calculated for the radial-tangential plane. An example of a calculated growth layer is illustrated by the thicker red line in Fig 11. The point marked "Investigated point" shows the calculated distance $R(p, R_{i0})$, for R_{i0} and p as marked in Fig 11. The tangent direction of $R(p, R_{i0})$ for the displayed example is represented by a solid black line. Thus, this line represents the determined fiber direction at the investigated point.

To determine, on the basis of laboratory data obtained using the scanner, growth layer surfaces corresponding to those calculated on the basis of Eq (5), bilinear interpolation between fiber directions determined in neighboring positions was used. The procedure can be described as follows: from a predefined starting point, a step of 0.1 mm was taken in the interpolated fiber direction. At the new point, a new interpolated fiber direction was determined and a new step was taken in this direction. This process was repeated until the boundary of the knot was reached. The linear interpolation was performed as

$$f(y,z) = \frac{\begin{bmatrix} y_2 - y & y - y_1 \end{bmatrix}}{(y_2 - y_1)(z_2 - z_1)} \cdot \begin{bmatrix} f(y_1, z_1) & f(y_1, z_2) \\ f(y_2, z_1) & f(y_2, z_2) \end{bmatrix} \cdot \begin{bmatrix} z_2 - z \\ z - z_1 \end{bmatrix}, \quad (6)$$

where $f(y,z)$ is the interpolated fiber angle for coordinate (y,z), and $f(y_1,z_1)$, $f(y_2,z_1)$, $f(y_1,z_2)$, and $f(y_2,z_2)$ are the closest measured angles in the grid.

Figure 12(a-c) show modeled knot boundaries and growth layer surfaces/curves (red lines) determined in three different ways, along with the fiber directions that are determined on the basis of laser scanning (black lines). Figure 12(a) shows growth layer surfaces calculated on the basis of Eq (6), whereas Fig 12(b) shows growth layer surfaces calculated on the basis of Eq (5). For both cases, the boundaries of the knot were defined as described in Knot Boundary section. By comparing the growth layer surfaces (Fig 12[a] and [b], respectively), one can see that the resemblance is rather good. This indicates that the measured fiber direction and the fiber direction calculated according to Eq (5) in the live knot region agree well with measured fiber directions.

When determining the knot geometry on the basis of laser scans of sawn timber, only data of the surface are obtained. The geometry of knots of the interior of the board is unknown. In such situations, an approximation of the knot volume must be based on some assumptions, and one such assumption/approximation would be to model the knot volume as a cone with an inclination from the pith and outward (see eg

Kandler et al 2016). The thinner red lines in Fig 12(c) show such a linear approximation of the part of the knot displayed. Using this knot geometry, together with Eq (5), results in the growth layer surfaces displayed in the same figure. Here, one can see that the resemblance between Fig 12 (a) and (c) is significantly lower than when comparing Fig 12(a) and (b).

Figure 12(d) and (e) show the difference in angle (absolute value) between measured fiber direction at certain positions and fiber direction calculated by Eq (5) for the same positions. The knot boundaries used for Fig 12(d) and (e) are the same as those shown in Fig 12(b) and (c), respectively. For the area just outside the dead part of the knot (marked in Fig 7[c]), the difference in angle is

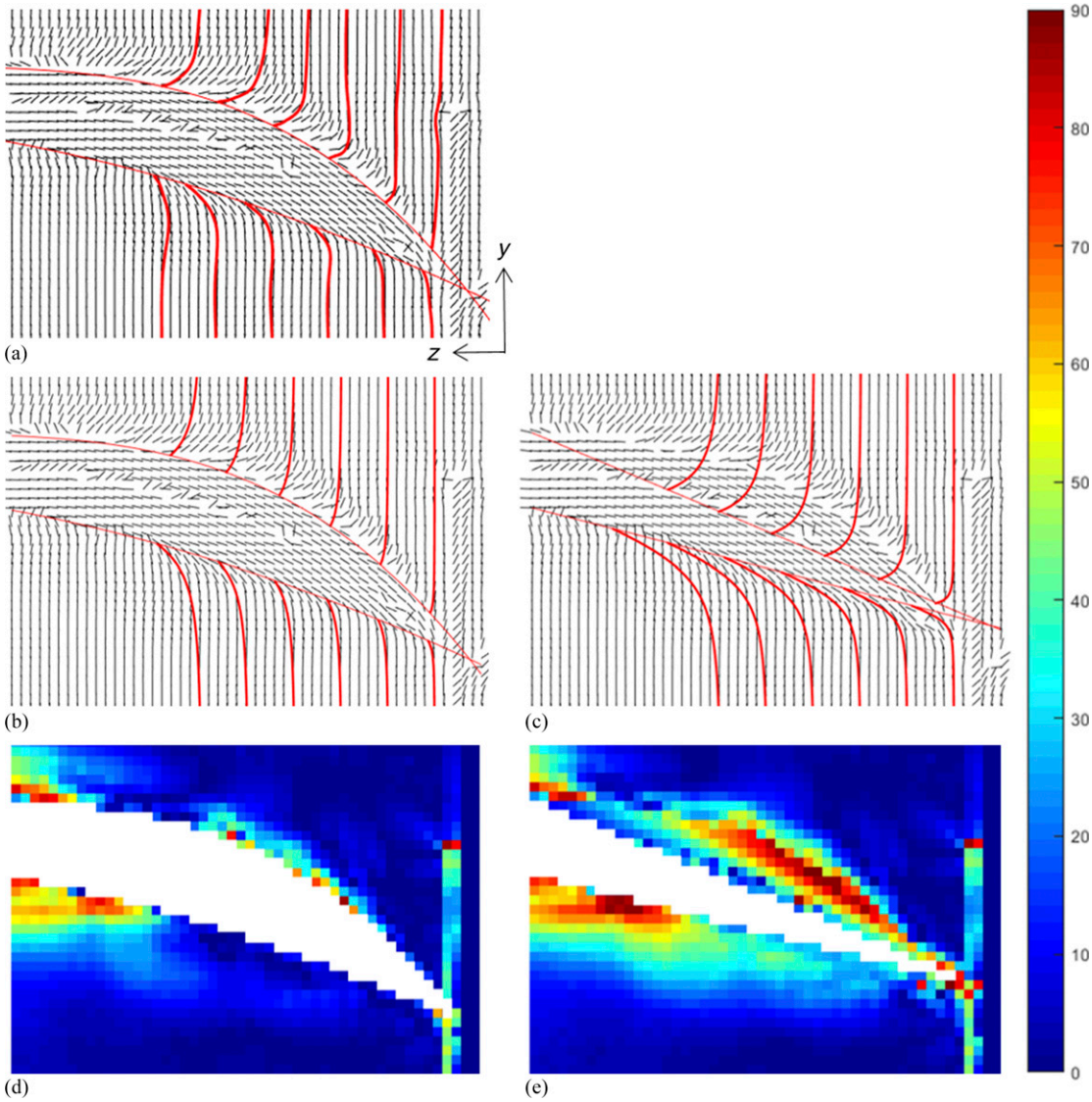

Figure 12. (a-c) Knot boundaries and growth layer surfaces (red lines) and fiber directions from laser scanning (black lines). (a and b) Knot boundaries as defined in the Knot Boundary section and (c) knot boundaries assuming a conical shape of the knot. (d and e) Difference of measured and calculated local fiber angles (degrees) assuming knot boundaries as defined in the Knot Boundary section and a conical knot shape, respectively.

generally more than 50°, as could be expected because Eq (5) is not valid for the dead part of the knot. In the vicinity of the live part of the knot, and if the knot boundaries are modeled as shown in Fig 12(a) and (b), the difference in angle is rather low, especially below the knot, see Fig 12 (d). However, if the knot boundaries are modeled as shown in Fig 12(c), the difference in angle in the live knot region increases significantly.

DISCUSSION AND CONCLUSION

It is a well-known fact that there is a strong relationship between fiber direction and strength, and between fiber direction and modulus of elasticity (Hankinson 1921; Hatayama 1984). An increased angle between load direction and fiber direction results in a decreased strength and stiffness. Even so, it is not until recently that such information has been implemented in machine strength grading applications, see eg Olsson and Oscarsson (2017) and Viguier et al (2017). In these two investigations, newly developed strength-grading methods are presented and both of them make use of the so-called tracheid effect to determine the in-plane angle of fibers on board's surfaces, whereas the out-of-plane angle (diving angle) is disregarded. Previous research has, however, shown that there is a relationship between the shape of the reflected laser light (shape factor ratio) and diving angle for an illuminated point on wood surfaces of silver birch and Scots pine (Simonaho et al 2004). If a sufficiently strong relationship exists between shape factor ratio and diving angle for Norway spruce, and if this relationship is valid for wood in the surroundings of knots, it would mean that the true 3D fiber direction on board surfaces could be determined solely by using the tracheid effect, and then be applied eg for further improvement of the strength-grading methods mentioned earlier.

In the research presented in this article, a newly developed laboratory scanner was used to measure both the in-plane fiber direction and the shape factor ratio on a specimen containing a single knot. It was assumed that the specimen had a plane of symmetry which contained both the pith of the knot and the pith of the tree. After splitting the specimen along this plane of symmetry, dot laser illumination was carried out on orthogonal planes.

The sampled data were used to investigate the relationship between *shape factor ratio* and *diving angle* in Norway spruce, and it was found that the relationship between these two entities is rather weak. It was also observed that the size of reflected laser light, as well as the shape factor ratio, differs between earlywood and latewood, which may be one of the explanations for the weak correlation. Another explanation is that the size of the reflected laser light on clear wood was approximately 10×5 mm in the fiber direction and in the fibers transverse direction, respectively. A similar size of the reflected light spot in the fiber direction is also reported by Nyström (2003). When illuminating the close surrounding of a knot, fibers both within and outside the knot will reflect light, and thus not enter the shape of an ellipse. This means that a resolution of 10×5 mm is actually insufficient to thoroughly investigate the relationship for the narrow transition zone between clear wood and knots. Improvements may be achieved if the size of the reflected laser light only covers a smaller area, ie if the light intensity is decreased and the in-plane fiber direction can still be determined with certainty. Further work on this should be carried out. Another remaining challenge when scanning full size timber is, however, that surfaces will then contain both round knots and splay knots and everything in between. Because the relationship between shape factor ratio and diving angle is probably quite different in the surroundings of knots that are cut in different planes, this is another source of uncertainty when it comes to application on full size timber.

The sampled data were also used to compare the mathematical equation given by Foley (2003) for the radial-longitudinal fiber direction in the vicinity of a live knot region. The resemblance between calculated fiber direction and measured fiber direction was good. This mathematical equation is, however, sensitive for the geometry of the knot. An erroneously defined knot geometry will lead to inaccurate calculated fiber direction.

Tracheid effect scanning gives reliable data of in-plane fiber directions on timber surfaces but not, as it seems, of diving angles. The shape factor ratio helps, however, to indicate where knots are located. The model presented by Foley (2003) give, on the other hand, information of fiber direction in 3D in the surroundings of knots, but only if the geometry of the knots that governs the fiber direction is known in detail. Further research, aiming at detailed knowledge of fiber direction for application on strength grading, should therefore combine data from scanning with application of a model of 3D fiber direction in the surrounding of knots. In practice, this may involve an iterative procedure including the following, after an initial identification of knots on timber surfaces and estimation of knot geometry parameters (Briggert et al 2016b; Kandler et al 2016): 1) calculation of fiber direction, 2) comparison between calculated and actual in-plane fiber direction on timber surfaces, and 3) adjustment of knot geometry parameters. An alternative approach would be to determine the geometry of knots on the basis of computer tomography (CT). Equipment for this purpose is currently available only for scanning of entire logs, or for small wood specimens to be examined in laboratory. Still, CT scanning of small wood specimens containing knots should be carried out to gain further knowledge of fiber orientation in 3D in the transition zone between clear wood and a knot. A method to compute fiber directions in clear wood from CT scanning was presented already by Ekevad (2004).

REFERENCES

Åstrand E (1996) Automatic Inspection of Sawn Wood. Doctoral thesis, Report no. 424. Department of Electrial Engineering, Linköping, Sweden.

Briggert A, Hu M, Olsson A, Oscarsson J (2016a) Evaluation of three dimensional fibre orientation in Norway spruce using a laboratory laser scanner. In Proc. World Conference of Timber Engineering, August 22-25, Vienna, Austria.

Briggert A, Olsson A, Oscarsson J (2016b) Three-dimensional modelling of knots and pith location in Norway spruce boards using tracheid-effect scanning. Eur J Wood Wood Prod 74(5):725-739.

Dinwoodie JM (2000) Timber: Its nature and behavior, 2nd edition. Taylor & Francis, New York, NY.

Ekevad M (2004) Method to compute fiber directions in wood from computed tomography images. J Wood Sci 50: 41-46.

Foley C (2003) Modeling the effects of knots in structural timber. Doctoral thesis, Report TVBK-1027. Lund Institute of Technology, Lund, Sweden.

Goodman JR, Bodig J (1978) Mathematical model of the tension behavior of wood with knots and cross-grain. In Proc. 1st International Conference on Wood Fracture, August 14-16, Banff, AB, Canada.

Hankinson RL (1921) Investigation of crushing strength of spruce at varying angles of grain. Air Service Information Circular, 3(259), Material Section Report No. 130. US Air Service, Washington, DC.

Hatayama Y (1984) A new estimation of structural lumber considering the slope of grain around knots. Bulletin of the Forestry and the Forest Products Research Institute, No. 326:69-167, Japan (in Japanese).

Hu M, Olsson A, Johansson M, Oscarsson J, Serrano E (2016) Assessment of a three-dimensional fiber orientation model for timber. Wood Fiber Sci 48(4):1-20.

Hu M, Briggert A, Olsson A, Johansson M, Oscarsson J, Säll H (2017) Growth layer and fibre orientation around knots in Norway spruce: A laboratory investigation. Wood Sci Technol 52(1):7-27.

Kandler G, Füssl J, Serrano E, Eberhardsteiner J (2015) Effective stiffness prediction of GLT beams based on stiffness distributions of individual lamellas. Wood Sci Technol 49:1101-1121.

Kandler G, Lukacevic M, Füssl J (2016) An algorithm for the geometric reconstruction of knots within timber boards based on fibre angle measurements. Constr Build Mater 124:945-960.

Lukacevic L, Füssl J (2014) Numerical simulation tool for wooden boards with a physically based approach to identify structural failure. Eur J Wood Wood Prod 72: 497-508.

Matthews PC, Beech BH (1976) Method and apparatus for detecting timber defects. U.S. Patent no. 3976384.

Nyström J (2003) Automatic measurement of fiber orientation in softwoods by using the tracheid effect. Comput Electron Agric 41:91-99.

Olsson A, Oscarsson J (2014) Three dimensional fibre orientation models for wood based on laser scanning utilizing the tracheid effect. In Proc. World Conference on Timber Engineering, August 10-14, Quebec, Canada.

Olsson A, Oscarsson J (2017) Strength grading on the basis of laser scanning and dynamic excitation: A full scale investigation of performance. Eur J Wood Wood Prod 75(1):17-31.

Olsson A, Oscarsson J, Serrano E, Källsner B, Johansson M, Enquist B (2013) Prediction of timber bending strength and in-member cross-sectional stiffness variation

on the basis of local wood fibre orientation. Eur J Wood Wood Prod 71(3):319-333.

Petersson H (2010) Use of optical and laser scanning techniques as tools for obtaining improved FE-input data for strength and shape stability analysis of wood and timber. In Proc. V European Conference on Computational Mechanics, May 16-21, Paris, France.

Philips GE, Bodig J, Goodman JR (1981) Flow-grain analogy. Wood Fiber Sci 14(2):55-65.

Shigo AL (1997) A new tree biology: Facts, photos and philosophies on trees and their problems and proper care. Eight Printing, Shigo and Trees, Durham, NE.

Simonaho S-P, Palviainen J, Tolonen Y, Silvennoinen R (2004) Determination of wood grain direction from laser light scattering pattern. Opt Lasers Eng 41:95-103.

Soest J, Matthews P, Wilson B (1993) A simple optical scanner for grain defects. Proc. 5th International Conference on Scanning Technology & Process Control for the Wood Products Industry, October 25-27, Atlanta, GA.

Viguier J, Bourreau D, Bocquet J-F, Pot G, Bléron L, Lanvin J-D (2017) Modelling mechanical properties of spruce and Douglas fir timber by means of X-ray and grain angle measurements for strength grading purpose. Eur J Wood Wood Prod 75:527-541.